P Vectors as a Diagnostic Tool for Synoptic-Scale Circulations

HUNG-CHI KUO

Department of Atmospheric Science, National Taiwan University, Taipei, Taiwan

WENDELL A. NUSS

Department of Meteorology, Naval Postgraduate School, Monterey, California

(Manuscript received 3 January 1994, in final form 14 June 1994)

ABSTRACT

The quasigeostrophic geopotential tendency equation is derived using *P* vectors in both pressure and entropy coordinates. This vector form of the geostrophic forcing in the geopotential tendency equation is similar to the *Q*-vector form of the ω equation. It is shown that the horizontal components of **P** are the advection of geostrophic momentum, and the vertical component of **P** is the horizontal temperature advection. The *P* vectors are shown to be related to *Q* and *C* vectors, as well as the ageostrophic circulation. The three-dimensional pseudocurl of the *P* vector gives the *C* vector that equals the ageostrophic pseudovorticity in the quasigeostrophic model. The horizontal components of the pseudocurl of **P** are perpendicular and proportional to the **Q**. The horizontal divergence of the *P* vector is the geostrophic absolute vorticity advection while the three-dimensional divergence of the *P* vector is the geostrophic quasigeostrophic potential vorticity advection. The ageostrophic wind can be partitioned into the *P* vector (geostrophic advective) and isallobaric wind contributions.

A numerical simulation of an idealized cyclone is used to characterize the distribution of the *P* vectors and *P*-vector diagnostics in order to demonstrate their potential application to the diagnosis of synoptic-scale circulations. The distribution of the *P* vectors clearly indicates the advections of geostrophic momentum and temperature that characterize cyclogenesis. An examination of the *P* vectors and the isallobaric wind demonstrates that the *P* vectors provide insight into the ageostrophic circulation of the cyclone. Diagnoses of the three-dimensional *P*-vector divergence and curl are shown to produce useful depictions of cyclonic vortex spinup and the propagation of both the large- and smaller-scale features of the system. These diagnostics can be interpreted from a variety of perspectives, including the height tendency and the advection of quasigeostrophic potential vorticity. The use of *P* vectors to diagnose synoptic-scale circulations appears to provide potentially useful insights into the dynamics of synoptic-scale disturbances not readily obtained from other diagnoses.

1. Introduction

Quasigeostrophic theory still provides the primary conceptual model used by synoptic meteorologists to understand the current weather as well as to evaluate numerical model forecasts. Quasigeostrophic theory is often summarized by the application of the geopotential tendency and omega equations (e.g., Holton 1979). The usual forms of both these equations contain two primary forcing terms, which are not independent and make physical interpretation difficult. Since quasigeostrophic theory is so widely applied as a conceptual model, it is useful to find good methods to extract the most physically meaningful information from quasigeostrophic diagnostics.

The divergence of the so-called *Q* vector was introduced by Hoskins et al. (1978) and Hoskins and Pedder (1980) as a simple, concise, one-term representation of the geostrophic forcing in the omega equation. Hoskins et al. (1978) and Hoskins and Pedder (1980) have an excellent discussion on the physical meaning of *Q* vectors. The two-dimensional *Q* vector provides a vectorial view of the geostrophic forcing of horizontal ageostrophic motion, and the divergence of the *Q* vector indicates the intensity of the vertical circulations. A chief advantage of the use of *Q* vectors over the traditional form of the omega equation for synoptic meteorologists is the relative ease by which both the horizontal and vertical ageostrophic motion can be deduced. In addition, their relationship to frontogenetical regions of the atmosphere provides an important link between frontal and larger-scale baroclinic wave circulations. This latter relationship is highlighted in Keyser et al. (1992), who considered the along- and cross-isentropic components of the *Q* vector to separate the vertical motion into cellular and banded patterns. The cellular pattern occurred on the scale of the baroclinic disturbance, and the banded pattern occurred on the scale of the embedded frontal zones. Xu

Corresponding author address: Dr. Wendell A. Nuss, Department of Meteorology, Naval Postgraduate School, Monterey, CA 93943-5100.

(1992) extends the Q vector to three dimensions and introduces the C vector. While the horizontal components of the C vector are essentially the same as the Q vector (with 90° rotation), the third component of the C vector is the vertical component of the ageostrophic pseudovorticity. This ageostrophic vorticity can be interpreted as the generation (rate) of the vertical curl of the Coriolis force due to the local geostrophic wind deformation and rotation. Xu and Keyser (1993) show that the vertical component of the ageostrophic pseudovorticity can be significant in a nonlinearly developing three-dimensional baroclinic wave or synoptic-scale cyclone.

In these studies, the vectorial view of the geostrophic forcing in the ω equation (or the ageostrophic circulation) is emphasized, although the geopotential tendency implications can be inferred and are briefly discussed. To complement this vectorial view of the omega equation, we present the geostrophic forcing of the geopotential tendency equation in terms of the P vector in this paper. The P vector was first introduced by Schubert (1985) in the derivation of the geopotential tendency equation in semigeostrophic theory. However, Schubert (1985) gave no physical explanation of the P vector. In this paper, the P vector in the simpler quasigeostrophic context is derived and its physical interpretation is discussed. In addition, the relationship between the P, the Q, and the C vectors, as well as the three-dimensional ageostrophic circulation are examined. The P-vector diagnostics are applied to an idealized synoptic-scale cyclone to demonstrate their potential use in synoptic meteorology. Section 2 presents the derivation of the quasigeostrophic P vector in pressure and entropy coordinates as well as the original semigeostrophic coordinates. Also discussed is a general physical interpretation of the P vector. Section 3 applies this form of the quasigeostrophic geopotential tendency equation to an idealized example of midlatitude cyclogenesis to characterize the distribution of the P vectors as well as derived P-vector diagnostics for a well-known synoptic-scale circulation. Section 4 summarizes the results and gives some concluding remarks.

2. Mathematical theory of P vectors

a. *Quasigeostrophic P vector in p coordinates on β plane*

Schubert (1985) first defined the P vector in semigeostrophic coordinates on an f plane. By analogy, if the hydrostatic and geostrophic balance relationships in pressure coordinates are used,

$$\left(f_0 u_g, f_0 v_g, \frac{RT}{p}\right) = \left(-\frac{\partial\Phi}{\partial y}, \frac{\partial\Phi}{\partial x}, -\frac{\partial\Phi}{\partial p}\right), \quad (2.1)$$

the P vector in pressure coordinates on β plane can be defined as

$$\mathbf{P} = (P_1, P_2, P_3)^{\mathrm{T}} = \left(\frac{\partial \mathbf{V}_g}{\partial x}\cdot\nabla_H\Phi - \beta y\frac{\partial\Phi}{\partial y}, \frac{\partial \mathbf{V}_g}{\partial y}\times\nabla_H\Phi - \beta y\frac{\partial\Phi}{\partial x}, -\frac{f_0^2}{\sigma}\frac{\partial \mathbf{V}_g}{\partial p}\cdot\nabla_H\Phi\right)^{\mathrm{T}}, \quad (2.2)$$

where $\mathbf{V}_g$ is the geostrophic wind vector, ∇_H the horizontal gradient operator on a pressure surface, $\sigma = -\alpha d\ln\theta_0/dp$, and θ_0 is the potential temperature corresponding to the basic-state temperature T_0.

Since $\mathbf{V}_g\cdot\nabla_H\Phi = 0$, the following identity holds for either the x, y, and p derivatives (denoted by $\partial/\partial x_i$):

$$\frac{\partial \mathbf{V}_g}{\partial x_i}\cdot\nabla_H\Phi = -\mathbf{V}_g\cdot\nabla\frac{\partial\Phi}{\partial x_i}. \quad (2.3)$$

With the help of (2.3) and (2.1), (2.2) can also be expressed as

$$\mathbf{P} = \left(-f_0\mathbf{V}_g\cdot\nabla_H v_g - \beta y\frac{\partial\Phi}{\partial y}, f_0\mathbf{V}_g\cdot\nabla_H u_g - \beta y\frac{\partial\Phi}{\partial x}, -\frac{f_0^2 R}{\sigma p}\mathbf{V}_g\cdot\nabla_H T\right)^{\mathrm{T}}. \quad (2.4)$$

From this form of the P vector it is evident that the horizontal components of $\mathbf{P}$ relate to the geostrophic advection of geostrophic momentum plus some β advection corrections, and the vertical component of $\mathbf{P}$ relates to the geostrophic advection of temperature on a constant pressure surface.

Using (2.4) and assuming that the flow is frictionless and adiabatic, the β-plane quasigeostrophic momentum and thermodynamic equations can be written using $\mathbf{P}$ as

$$D_g u_g = \frac{\partial u_g}{\partial t} + \frac{1}{f_0}P_2 = f_0 v_a, \quad (2.5)$$

$$D_g v_g = \frac{\partial v_g}{\partial t} - \frac{1}{f_0}P_1 = -f_0 u_a, \quad (2.6)$$

$$D_g T = \frac{\partial T}{\partial t} - \frac{p}{R}\frac{\sigma}{f_0^2}P_3 = -\frac{\sigma p}{R}\omega, \quad (2.7)$$

where $D_g = \partial/\partial t + \mathbf{V}_g\cdot\nabla_H$. Equations (2.1), (2.5)–(2.7), and the continuity equation

$$\frac{\partial u_a}{\partial x} + \frac{\partial v_a}{\partial y} + \frac{\partial\omega}{\partial p} = 0 \quad (2.8)$$

constitute a closed set of equations with u_g, v_g, u_a, v_a, T, ω, and Φ as variables. Although both friction and diabatic heating terms can be incorporated into the definitions of P_1, P_2, and P_3, the practical utility of doing so is significantly limited by our ability to quantify these diabatic terms.

Using the P vector and (2.1), the (2.5)–(2.7) can also be expressed in vectorial form as

$$\mathbf{V_a} = \frac{1}{f_0^2}(\mathbf{P} - \nabla_{f\sigma}\Phi_t), \tag{2.9}$$

where $\Phi_t = \partial\Phi/\partial t$, $\nabla_{f\sigma} = (\partial/\partial x)\mathbf{i} + (\partial/\partial y)\mathbf{j} + (f_0^2/\sigma)(\partial/\partial p)\mathbf{k}$, the three-dimensional gradient operator with the scaling factor of f_0^2/σ in the vertical spatial derivative, and $\mathbf{V}_a = (u_a, v_a, \omega)^{\mathrm{T}}$. Equation (2.9) suggests that the ageostrophic wind can be divided into a geostrophic advective contribution (P vector) and an isallobaric wind contribution. Lim et al. (1991) decomposed the ageostrophic wind into similar contributions but did not express the geostrophic advective contribution in terms of P vectors.

Utilizing the above equations, the derivation of the vorticity, geopotential tendency, ageostrophic circulation, and omega equations are straightforward. The x derivative of (2.6) minus the y derivative of (2.5) yields the quasigeostrophic vorticity equation

$$\frac{\partial\zeta_g}{\partial t} - \frac{1}{f_0}\left(\frac{\partial P_1}{\partial x} + \frac{\partial P_2}{\partial y}\right) = f_0\frac{\partial\omega}{\partial p}, \tag{2.10}$$

where $\zeta_g = \partial v_g/\partial x - \partial u_g/\partial y$ the geostrophic vorticity. Equation (2.10) reveals that $-\mathbf{V_g}\cdot\nabla_H(\zeta_g + f) = f_0^{-1}(\partial P_1/\partial x + \partial P_2/\partial y)$, which implies that the horizontal divergence of $\mathbf{P}$ is equal to the horizontal geostrophic absolute vorticity advection. By taking the divergence of (2.9) and using the continuity equation (2.8), the geopotential tendency equation is obtained with the three-dimensional divergence of $\mathbf{P}$ on the right-hand side:

$$(\nabla\cdot\nabla_{f\sigma})\Phi_t = \left[\nabla_H^2 + \frac{\partial}{\partial p}\left(\frac{f^2}{\sigma}\frac{\partial}{\partial p}\right)\right]\Phi_t = \nabla\cdot\mathbf{P}, \tag{2.11a}$$

where ∇_H^2 denotes the horizontal Laplacian operator and ∇ the three-dimensional gradient operator. At the top and bottom of the atmosphere (or domain), the geopotential tendency equation must fit the following vertical boundary conditions:

$$\frac{f_0^2}{\sigma}\frac{\partial\Phi_t}{\partial p} = P_3. \tag{2.11b}$$

These Neumann-type boundary conditions come from applying the thermodynamic equation (2.7) at the bottom and top of the domain and are consistent with imposing a condition that ω vanish at the upper and lower boundaries. Consequently, (2.11) indicates that the geopotential tendency is proportional to the divergence of $\mathbf{P}$ in the *interior* of domain.

An alternative interpretation of the three-dimensional divergence of $\mathbf{P}$ is obtained by comparing (2.11a) to the well-known quasigeostrophic potential vorticity equation

$$\frac{\partial q}{\partial t} = -\mathbf{V}_g\cdot\nabla_H q, \tag{2.12a}$$

$$q = \nabla_H^2\Phi + \frac{\partial}{\partial p}\left(\frac{f^2}{\sigma}\frac{\partial\Phi}{\partial p}\right). \tag{2.12b}$$

From this comparison, the divergence of $\mathbf{P}$ is seen to be the geostrophic advection of quasigeostrophic potential vorticity [right-hand side of (2.12a)].

Equations (2.1), (2.2), and (2.11) form a closed set of quasigeostrophic equations with the variables $\mathbf{P}$ and Φ. The P vector can be computed from Φ using (2.1) and (2.2), from which the geopotential tendency Φ_t can be diagnosed using (2.11). The ageostrophic wind vector $\mathbf{V}_a$ need not be directly evaluated. However, $\mathbf{V}_a$ can be obtained using (2.9) with the distribution of the P vector and either the observed isallobaric winds or the solution for the geopotential tendency Φ_t in (2.11).

The relationship between P, Q, and C vectors and the ageostrophic circulations can also be determined from (9) with the help of the identity $\nabla_{f\sigma}\times\nabla_{f\sigma}\Phi_t = 0$. Taking $\mathbf{k}\times[\sigma\nabla_{f\sigma}\times(2.9)]$, we have the Q vector [which is the same as the horizontal component of the C vector with 90° rotation (Xu 1992)]

$$-2\mathbf{Q} = 2\mathbf{k}\times\mathbf{C} = \mathbf{k}\times(\sigma\nabla_{f\sigma}\times\mathbf{V_a}) = \mathbf{k}\times\left(\frac{\sigma}{f_0^2}\nabla_{f\sigma}\times\mathbf{P}\right), \tag{2.13a}$$

and taking $\mathbf{k}\cdot[\nabla_{f\sigma}\times(2.9)]$, we have the vertical component of $\mathbf{C}$ and the ageostrophic pseudovorticity

$$2C_3 = f_0^2\left[\frac{\partial}{\partial x}v_a - \frac{\partial}{\partial y}u_a\right] = \frac{\partial}{\partial x}P_2 - \frac{\partial}{\partial y}P_1. \tag{2.13b}$$

Equation (2.13a) can also be put in scalar form:

$$\nabla_H(\sigma\omega) - f_0^2\frac{\partial}{\partial p}\begin{pmatrix}u_a\\ v_a\end{pmatrix} = \nabla_H\left(\frac{\sigma}{f_0^2}P_3\right) - \frac{\partial}{\partial p}\begin{pmatrix}P_1\\ P_2\end{pmatrix} = -2\mathbf{Q}, \tag{2.14}$$

where

$$\mathbf{Q} = (Q_1, Q_2) = \frac{-R}{p}\left(\frac{\partial\mathbf{V_g}}{\partial x}\cdot\nabla_H T, \frac{\partial\mathbf{V_g}}{\partial y}\cdot\nabla_H T\right). \tag{2.15}$$

With the scaling factors of f_0 and σ, (2.14) indicates that the horizontal component of the curl of $\mathbf{P}$ is perpendicular and proportional to $\mathbf{Q}$. Since Q vectors point perpendicular to the instantaneous axis along which the temperature gradient is contracting (frontogenesis), it is evident that the curl of $\mathbf{P}$ points along this axis of temperature gradient contraction. This implies that for a simple two-dimensional frontal situation, both the P and Q vectors will point across

the front in the direction of the low-level ageostrophic flow, and the vertical component of the P vectors will point up or down depending upon the sign of the temperature advection.

b. Quasigeostrophic isentropic P vector on β plane

While the pressure coordinates are most commonly used in quasigeostrophic theory, potential temperature θ coordinates can also be used and provide additional insight into quasigeostrophic dynamics. For example, Berrisford et al. (1993) present the quasigeostrophic potential vorticity in isentropic (θ) coordinates and discuss the simple relationship between the quasigeostrophic potential vorticity and Ertel potential vorticity when isentropic coordinates are used. Results from Berrisford et al. (1993) are used in the following derivation of the isentropic P vector. However, to define the isentropic P vector similar to (2.2), an entropy vertical coordinate is used instead of the usual isentropic coordinate. The entropy s is defined as

$$s = c_p \ln\left(\frac{\theta}{\theta_0}\right) = c_p \ln\left(\frac{T}{T_0}\right) - R \ln\left(\frac{p}{p_0}\right), \quad (2.16)$$

where p_0, T_0, and θ_0 are constant reference values of pressure, temperature, and potential temperature.

Similar to (2.2), the isentropic $\mathbf{P}$ on β plane is

$$\mathbf{P} = \left(\frac{\partial \mathbf{V_g}}{\partial x} \cdot \nabla_{Hs} M - \beta y \frac{\partial M}{\partial y}, \frac{\partial \mathbf{V_g}}{\partial y} \times \nabla_{Hs} M - \beta y \frac{\partial M}{\partial x}, \frac{f_0^2}{\sigma^*} \frac{\partial \mathbf{V_g}}{\partial s} \cdot \nabla_{Hs} M\right)^{\mathrm{T}}, \quad (2.17)$$

where $M = gz + c_pT$ is the Montgomery potential, $\sigma^* = -(\rho_0 c_p)^{-1} dp_0/ds$, ∇_{Hs} is the horizontal gradient operator on an entropy surface, and the other variables take their usual meaning.

With the help of the geostrophic and hydrostatic balances in entropy coordinates

$$(f_0 u_g, f_0 v_g, T) = \left(-\frac{\partial M}{\partial y}, \frac{\partial M}{\partial x}, \frac{\partial M}{\partial s}\right) \quad (2.18)$$

and identities similar to (2.3) in entropy coordinates, the entropy counterpart of (2.4) is

$$\mathbf{P} = \left(-f_0 \mathbf{V_g} \cdot \nabla_{Hs} v_g - \beta y \frac{\partial M}{\partial y}, f_0 \mathbf{V_g} \cdot \nabla_{Hs} u_g - \beta y \frac{\partial M}{\partial x}, -\frac{f_0^2}{\sigma^*} \mathbf{V_g} \cdot \nabla_{Hs} T\right)^{\mathrm{T}}. \quad (2.19)$$

Similar to the pressure coordinate form of $\mathbf{P}$, the horizontal components of $\mathbf{P}$ relate to the geostrophic advection of geostrophic momentum plus some β corrections and the vertical component of $\mathbf{P}$ relates to the geostrophic advection of temperature. However, these advections are now calculated on constant entropy surfaces as opposed to pressure surfaces.

The frictionless, adiabatic, β-plane quasigeostrophic momentum equations in entropy coordinates can now be written using this P vector as

$$D_{gs} u_g = \frac{\partial u_g}{\partial t} + \frac{1}{f_0} P_2 = f_0 v_a, \quad (2.20)$$

$$D_{gs} v_g = \frac{\partial v_g}{\partial t} - \frac{1}{f_0} P_1 = -f_0 u_a, \quad (2.21)$$

where $D_{gs} = \partial/\partial t + \mathbb{V}_\mathbf{g} \cdot \nabla_{Hs}$. The isentropic vorticity equation can be derived from (2.20) and (2.21):

$$\frac{\partial \zeta_{gs}}{\partial t} - \frac{1}{f_0} \nabla_{Hs} \cdot \mathbb{P} + f_0 \left(\frac{\partial u_a}{\partial x} + \frac{\partial v_a}{\partial y}\right) = 0, \quad (2.22)$$

where $\zeta_{gs} = (\partial v_g/\partial x - \partial u_g/\partial y)_s$ is the isentropic geostrophic vorticity. Equation (2.22) reveals that $-\mathbf{V_g} \cdot \nabla_H (\zeta_{gs} + f) = f_0^{-1} \nabla_{Hs} \cdot \mathbb{P}$, which is the isentropic counterpart of (2.10). This equation indicates that the horizontal divergence of the isentropic $\mathbb{P}$ is equal to the horizontal isentropic geostrophic absolute vorticity advection.

Mass conservation in entropy coordinates under adiabatic conditions is

$$D_{gs} \frac{\partial p}{\partial s} + \frac{dp_0}{ds} \left(\frac{\partial u_a}{\partial x} + \frac{\partial v_a}{\partial y}\right) = 0, \quad (2.23)$$

and in an approximate form can be used to derive a Montgomery potential tendency equation using P vectors. Within the quasigeostrophic context, as has been discussed in Berrisford et al. (1993), p and T are related by

$$\frac{T}{T_0} \approx \kappa \frac{p}{p_0}, \quad (2.24a)$$

or

$$\rho_0 c_p T \approx p. \quad (2.24b)$$

Using the relationships of (2.24) in (2.23) and the definition of P_3 in (2.19), an approximate form of the mass conservation equation is

$$D_{gs} \frac{\partial T}{\partial s} - \sigma^* \left(\frac{\partial u_a}{\partial x} + \frac{\partial v_a}{\partial y}\right) = \frac{\partial}{\partial t} \frac{\partial T}{\partial s} - \frac{\sigma^*}{f_0^2} \frac{\partial P_3}{\partial s} - \sigma^* \left(\frac{\partial u_a}{\partial x} + \frac{\partial v_a}{\partial y}\right) = 0, \quad (2.25)$$

where ρ_0 and σ^* are taken to be slowly varying functions of s.

The Montgomery potential tendency equation using P vectors is obtained by canceling the $\partial u_a/\partial x + \partial v_a/\partial y$ term in (2.22) and (2.25) and using the hydrostatic balance relationship. The result is the isentropic counterpart of (2.11),

$$\left(\nabla_{Hs}^2 + \frac{f_0^2}{\sigma^*}\frac{\partial^2}{\partial s^2}\right) M_t = \nabla_s \cdot \mathbf{P} \tag{2.26a}$$

or

$$\frac{\partial}{\partial t}\left(\nabla_{Hs}^2\psi + \beta y + \frac{f_0^2}{\sigma^*}\frac{\partial^2\psi}{\partial s^2}\right) = \frac{1}{f_0}\nabla_s \cdot \mathbf{P}, \tag{2.26b}$$

where ∇_{Hs}^2 denotes the horizontal isentropic Laplacian operator, ∇_s the gradient operator in entropy coordinates, $M_t = \partial M/\partial t$, and the streamfunction $\psi = M/f_0$. The boundary conditions for (2.26a) and (2.26b) are

$$\frac{f_0^2}{\sigma^*}\frac{\partial M_t}{\partial s} = P_3 \tag{2.26c}$$

or

$$\frac{f_0^2}{\sigma^*}\frac{\partial \psi_t}{\partial s} = \frac{P_3}{f_0}. \tag{2.26d}$$

Similar to the result obtained from (2.11) in pressure coordinates, (2.26) shows that $\nabla_s \cdot \mathbf{P}$ is equivalent to the geostrophic advection of isentropic quasigeostrophic potential vorticity as well as the geostrophic forcing of Montgomery potential tendencies.

c. *Semigeostrophic P vector in geostrophic coordinates*

The extensions of the derivations using P vectors in the previous sections to the semigeostrophic system are straightforward and have been previously described by Schubert (1985). With the usual notations for semigeostrophic equations using the pseudoheight coordinate $Z = [1 - (p/p_0)^\kappa]c_p\theta_0/g$, the generalization involves replacing independent variables (x, y) by the geostrophic coordinate (absolute angular momentum) $(X, Y) = (x + v_g/f_0, y - u_g/f_0)$, σ by the Ertel potential vorticity q^*, Φ by the potential function $\Phi^* = \Phi + (u_g^2 + v_g^2)/2$, and $\mathbf{V_a}$ by $\mathbf{V_a^*}$ (Hoskins and Draghici 1977). The transformed ageostrophic components of $\mathbf{V_a^*}$ are

$$(u_a^*, v_a^*, w^*) = \left(u_a + \frac{w}{f_0}\frac{\partial v_g}{\partial Z}, v_a - \frac{w}{f_0}\frac{\partial u_g}{\partial Z}, \frac{f_0}{\zeta}w\right), \tag{2.27}$$

where ζ is the absolute vorticity. In the Boussinesq atmosphere, $\mathbf{V_a^*}$ satisfies the continuity equation

$$\frac{\partial u_a^*}{\partial X} + \frac{\partial v_a^*}{\partial Y} + \frac{\partial w^*}{\partial Z} = 0. \tag{2.28}$$

Consequently, $\mathbf{P}$ in semigeostrophic theory is defined as

$$\mathbf{P} = \left(\frac{\partial \mathbf{V_g}}{\partial X}\cdot\nabla_H\Phi^*, \frac{\partial \mathbf{V_g}}{\partial Y}\cdot\nabla_H\Phi^*, \frac{f_0^2}{q^*}\frac{\partial \mathbf{V_g}}{\partial Z}\cdot\nabla_H\Phi^*\right)^{\mathrm{T}}, \tag{2.29}$$

and the semigeostrophic counterparts of (2.5)–(2.7) are

$$\frac{\partial u_g}{\partial t} + \frac{1}{f_0}P_2 = f_0 v_a^*, \tag{2.30a}$$

$$\frac{\partial v_g}{\partial t} - \frac{1}{f_0}P_1 = -f_0 u_a^*, \tag{2.30b}$$

$$\frac{\partial}{\partial t}\left(\frac{g}{\theta_0}\theta\right) - \frac{q^*}{f_0^2}P_3 = -q^* w^*, \tag{2.30c}$$

where the time derivative is in the geostrophic coordinate. Analogous equations for the ageostrophic velocity (2.9), the potential tendency (2.11), and the relationships between P, Q, and C vectors (2.13) can also be derived using the semigeostrophic P vector.

d. *Summary of P-vector relationships*

The mathematical relationships in the previous sections provide the basis by which P vectors can be used for the diagnosis of synoptic-scale circulations using quasigeostrophic theory. The most significant physical relationship indicated above is that the three-dimensional divergence of the P vector can be interpreted as either the geostrophic forcing of geopotential tendency or as the geostrophic advection of quasigeostrophic potential vorticity. Although the actual distribution of geopotential at some future time requires the solution of a three-dimensional elliptic equation, the distribution of the forcing or quasigeostrophic potential vorticity can still be physically enlightening. This is evident from studies such as Davis and Emanuel (1991), which suggest that approximate inversion of the potential vorticity can be used to determine the circulation. The other significant physical relationship indicated above is the relationship between the P vector, the isallobaric wind, and the ageostrophic wind. This relationship indicates that the P vector can be used to deduce the contributing factors to the ageostrophic circulation of synoptic scale systems. The P vector measures the contribution to the ageostrophic circulation due to the advection of geostrophic momentum. As illustrated in (2.9), the other contributing factor to the ageostrophic circulation is due to the isallobaric wind. As suggested by Lim et al. (1991), the magnitude of advective forcing tends to dominate at upper levels, while the two processes are of similar magnitude at lower levels. These relationships are explored more completely in the next section.

3. An application

To illustrate the potential application of P vectors to synoptic meteorology as well as demonstrate their basic characteristics, P-vector diagnostics were applied to a numerical model simulation of an idealized cyclone. This study uses numerical simulations made with the NCAR–Penn State mesoscale model of an idealized cyclone that has previously been described by Nuss and Anthes (1987). The choice of this idealized cyclone simulation is designed to illustrate the use of P vectors in a simplified synoptic-scale baroclinic wave to facilitate their physical interpretation. A diabatic simulation is used in order to demonstrate this diagnostic under realistic conditions. Future studies are planned to test the utility of this diagnostic when applied to arbitrary atmospheric circulations.

The idealized cyclone model simulation examined in this study utilized analytic initial conditions designed to generate an intense cyclone. The exact formulation of these initial conditions is described in detail in Nuss and Anthes (1987) and essentially consists of a zonal baroclinic jet with both a preexisting upper- and lower-level finite amplitude perturbation. The initial conditions were periodic in the east–west direction, and the model was run in a channel-flow mode with fixed north–south boundary conditions. The simulation examined in this study was a simulation with Kuo cumulus parameterization and the high-resolution boundary layer parameterization with no surface heat and moisture fluxes included. The model domain was 4000 km × 4000 km with a 100-km grid spacing. Specific details can be found in Nuss and Anthes (1987). Calculation of P vectors and all other diagnostics in this paper were done on the model grid using second-order, centered, finite-difference equations applied in pressure coordinates after the model sigma levels were interpolated to pressure levels.

To illustrate the distribution of P-vector diagnostics in a baroclinic cyclone, the model simulation was examined in detail at the 24-h point in the simulation. As illustrated in Fig. 1, the cyclone at 24 h in the simulation is an intense 983-mb low pressure center at the surface, which has distinct warm and cold fronts at this time. The surface fronts developed as the cyclone intensified from its initial central pressure of 1008 mb, which had no concentrated thermal gradients at the initial time. The upper-level wave has also amplified during the 24-h period as illustrated in Fig. 2, which has a vorticity maximum of 19×10^{-5} s^{-1} in the base of the trough. The lobe of strong cyclonic vorticity downstream from the primary trough was generated in response to the latent heat release along the surface warm front. Although the structure of this model simulation may not be characteristic of all actual cyclones, it contains

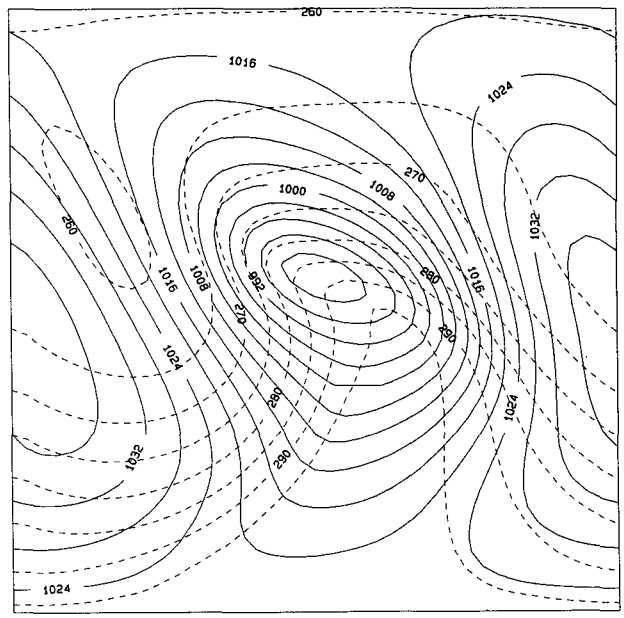

FIG. 1. Sea level pressure in (mb, solid) and surface temperature (K, dashed) at 24 h in the simulation. Pressure contour interval is 4 mb and temperature contour interval is 5 K.

the essential ingredients that characterize baroclinic cyclogenesis, including the diabatic effects due to latent heat release and surface friction. Although the adiabatic P-vector diagnosis that is applied in the following sections does not explicitly account for the diabatic effects, this application illustrates both the general characteristics of the P vectors as well as the information one is likely to obtain when applying P vectors to actual synoptic-scale analyses where diabatic processes are difficult to quantifiy.

a. P-vector distribution and interpretation

To begin to illustrate the use of P-vector diagnostics, the distribution of the P vectors was examined for the idealized cyclone. As discussed in the previous section, the horizontal components of the P vector correspond to the horizontal geostrophic advection of geostrophic momentum, and the vertical component of the P vector corresponds to the geostrophic thermal advection (2.2). Figure 3 displays the horizontal components of the P vectors at 500 mb, which shows that the P vectors point across the flow toward higher (lower) heights downstream (upstream) from the upper-level trough axis. This orientation of the P vectors indicates that the higher geostrophic momentum in the southwesterly flow downstream from the trough is being advected to the southeast, which is required for the eastward propagation of the wave. Likewise, the higher geostrophic momentum in the northwestly flow upstream from the trough is being ad-

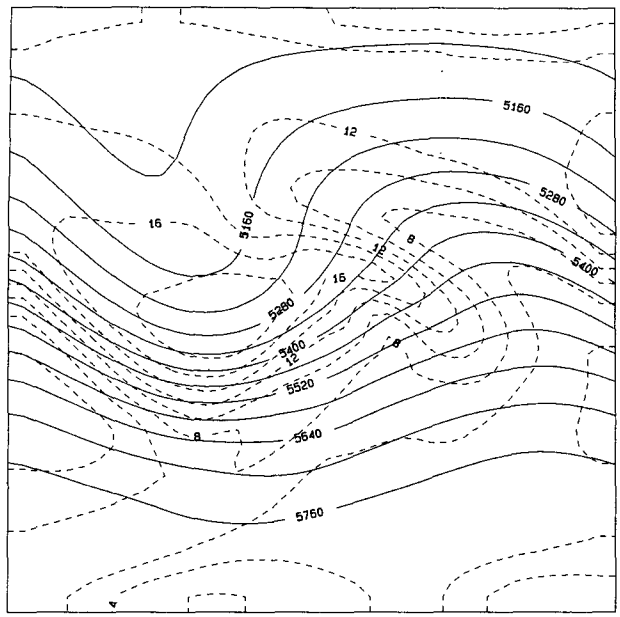

FIG. 2. The 500-mb geopotential height (m, solid) and absolute vorticity (10^{-5} s^{-1}, dashed) at 24 h in the simulation. Height contour interval is 60 m and vorticity contour interval is 2×10^{-5} s^{-1}.

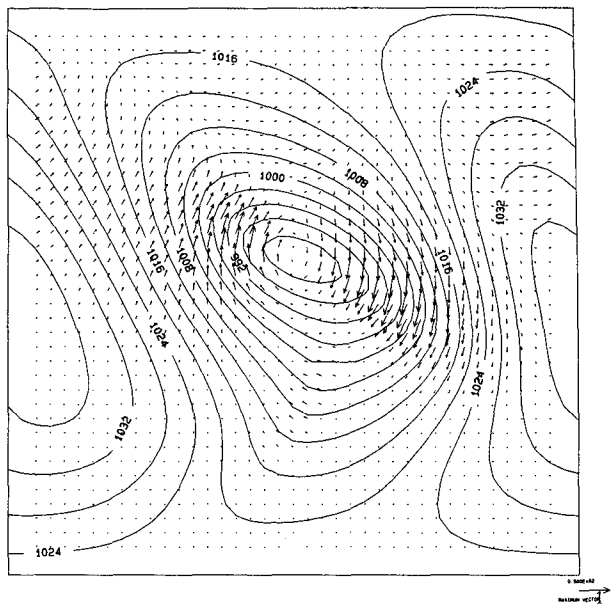

FIG. 4. As in Fig. 3 except for sea level pressure (mb, solid) every 4 mb and maximum vector corresponds to 50×10^{-8} m s^{-3}.

vected northeastward, which again is consistent with the eastward movement of the trough. Figure 4 displays the horizontal components of the P vectors at 950 mb (lowest level that could be computed) superimposed on the sea level pressure. Near the surface, the P vectors essentially point around the low pressure center in an anticyclonic direction. However, the pattern is not symmetric with the warm-frontal trough and the inverted trough to the northwest of the low center having the largest P vectors. These trough regions, as well as the cold-frontal trough to a lessor de-

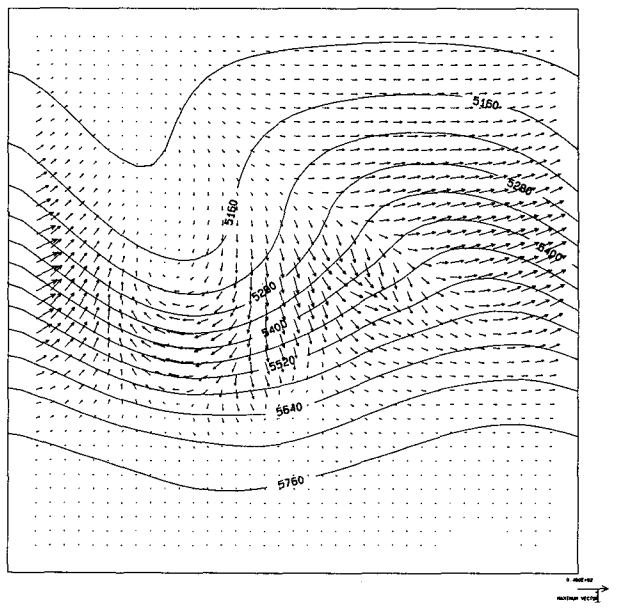

FIG. 3. The 500-mb geopotential height in (m, solid) and horizontal components of the P vector. Height contour interval as in Fig. 2. The P vectors are scaled according to magnitude. Maximum vector appears in lower right and corresponds to 40×10^{-8} m s^{-3}.

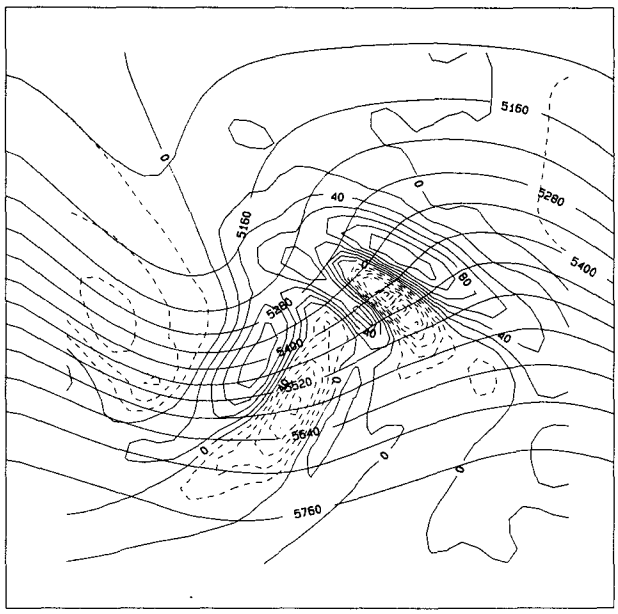

FIG. 5. The 500-mb geopotential height in (m, solid) and horizontal divergence of P vectors in 8.64×10^{13} s^{-2} (vorticity units per day). Solid lines correspond to cyclonic vorticity increases and dashed lines to cyclonic vorticity decreases.

gree, represent regions of enhanced geostrophic momentum advection that results from the rapid directional change in the geostrophic flow in these regions of enhanced curvature.

The interpretation of the horizontal components of the P vectors causing propagation of a trough is analogous to that obtained by considering the height changes forced by the geostrophic advection of geostrophic vorticity. Downstream (upstream) from an upper-level trough cyclonic (anticyclonic) geostrophic vorticity advection forces height falls (rises), assuming no other contributions to height tendency exist. This relationship is obtained mathematically by taking the horizontal divergence of the P vectors (2.10). When applied to the present case, the resultant vorticity advection patterns at 500 mb (Fig. 5) and sea level (not shown) indicate the tendency for the upper-level trough to propagate, as well as the low-level fronts to propagate. This interpretation is consistent with that obtained by considering only the vorticity forcing in the traditional form of the height tendency equation.

An alternative way of interpreting the horizontal components of the P vector is obtained by considering the vertical component of the curl of the P vector. This component is given in (2.13b) and is related to the vertical component of the C vector or the ageostrophic pseudovorticity (Xu 1992). Without actually calculating the curl, it is evident in Fig. 3 that the 500-mb trough is characterized by anticyclonic curl of the horizontal P-vector components. This implies that the ageostrophic pseudovorticity of the upper-level trough is anticyclonic, which is consistent with an induced ageostrophic flow that is attempting to restore geostrophic balance. Likewise, the surface low and frontal troughs have anticyclonic ageostrophic pseudovorticity, which is consistent with the tendency of the induced ageostrophic circulation to oppose the geostrophic advections. As shown by Xu (1992), the actual distribution of the ageostrophic flow can be obtained from this pseudovorticity given appropriate boundary conditions, whereas the P vectors alone are not sufficient as seen in (2.9). The isallobaric contribution to the ageostrophic flow must be known in addition to the P vectors to determine the actual ageostrophic vectors, which will be explored more completely below.

The vertical component of the P vectors is best seen by considering an west–east cross section through the developing cyclone. Figure 6 shows the vertical and horizontal component of the P vectors in the plane of the cross section. The vertical structure of the wave is evident in the potential temperature and the

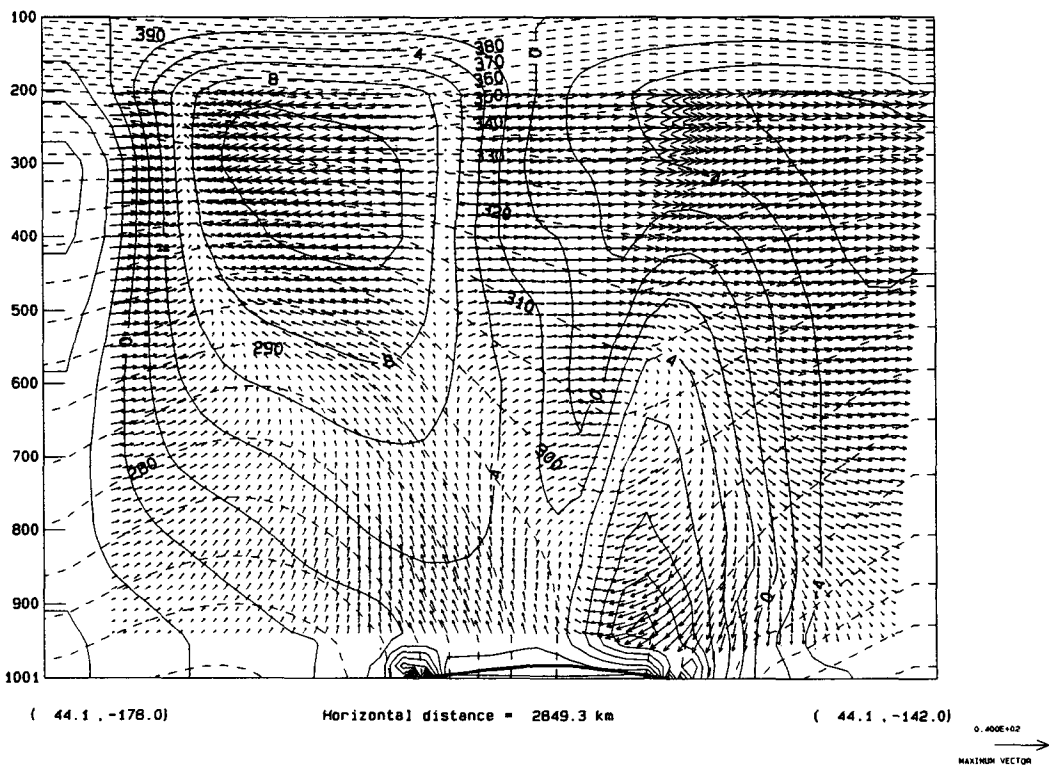

FIG. 6. West–east cross section of P vectors, potential temperature (K, dashed), and relative vorticity (solid and dashed) through the center of the cyclone at 24 h in the simulation. The P vectors scaled as in Fig. 4. Potential temperature is contoured every 5 K. Relative vorticity is contoured every 2×10^{-5} s^{-1}.

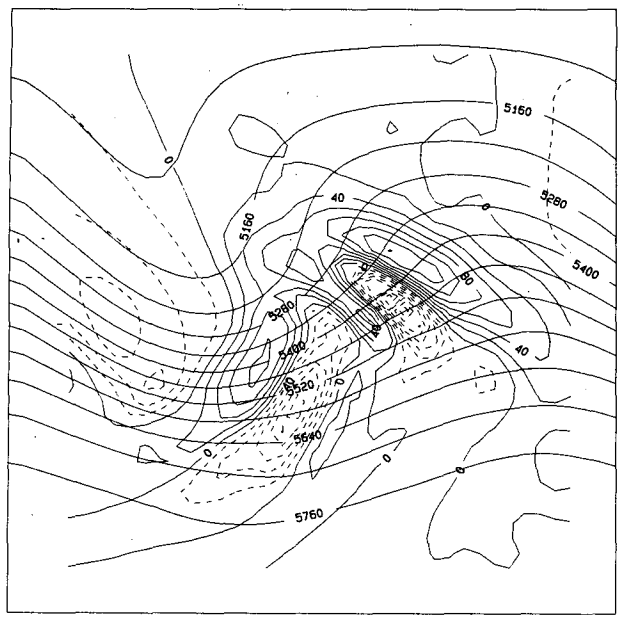

FIG. 7. The 500-mb geopotential height (m, solid) and three-dimensional divergence of P vectors in 1.5×10^{14} m s^{-1}, which is equivalent to meters per hour for a 4000-km-wavelength wave. Solid lines correspond to P-vector divergence and dashed lines to P-vector convergence.

relative vorticity fields shown on the cross section as well. The downward-directed P vectors to the east of the trough axis represent the region of warm thermal advection, and the upward-directed P vectors to the west indicate the cold thermal advection region. The differential thermal advection is easily deduced from the P-vector cross section and clearly shows that the thermal advections are strongest in the lower levels in this case. The eastward advection of geostrophic momentum to the east of the upper-level trough seen in the horizontal (Fig. 3) is evident on the cross section as well. Although the present diagnosis does not include the direct effects of diabatic heating, the impact of latent heat release on the vertical component of the P vector will be much the same as warm advection. Consequently, the downward-directed P vectors to the east of the surface low are likely to be larger in a diabatic formulation as a result of the latent heat release in this region of the cyclone.

b. *P-vector divergence diagnosis*

As stated in the previous section, $\nabla\cdot\mathbf{P}$ is related to the geostrophic forcing in the geopotential tendency (2.11), as well as the advection of quasigeostrophic potential vorticity advection (2.12). Both these relationships provide useful diagnostic insight into the developing cyclone example. The three-dimensional divergence of the P vectors is shown at the 500-mb level in Fig. 7. Interpreting the divergence of $\mathbf{P}$ as the forcing of the geopotential tendency, the character of the height tendencies at this level can be deduced by treating the three-dimensional Laplacian operator on the left-hand side of 2.11 as simply reversing the sign of the forcing. Consequently, positive values of the P-vector divergence correspond to regions of height falls and conversely for negative values of the P-vector divergence. To compute the actual height tendency requires that the Laplacian operator be inverted, which tends to smooth the distribution of height changes compared to the forcing distribution. However, the correspondence between the forcing and the maximum height changes is relatively good as can be seen in the distribution of the height changes over the 6-h period centered at the time of the forcing (Fig. 8). The region of largest height falls just downstream from the trough corresponds very closely to the large P-vector divergence just downstream from the trough. However, the observed height falls cover a broad region, while the P-vector divergence has considerably more structure. This difference is the result of not inverting the forcing (P-vector divergence) to obtain the predicted height tendency. However, the axis of strong forcing that is due to the impact of the latent heat along the warm front is evident as enhanced height falls in the broad region of observed height falls in Fig. 8. Although geostrophically deduced, the impact of the diabatic processes prior to this time is clearly evident in this region of P-vector divergence and the associated height tendency. A diagnosis that includes

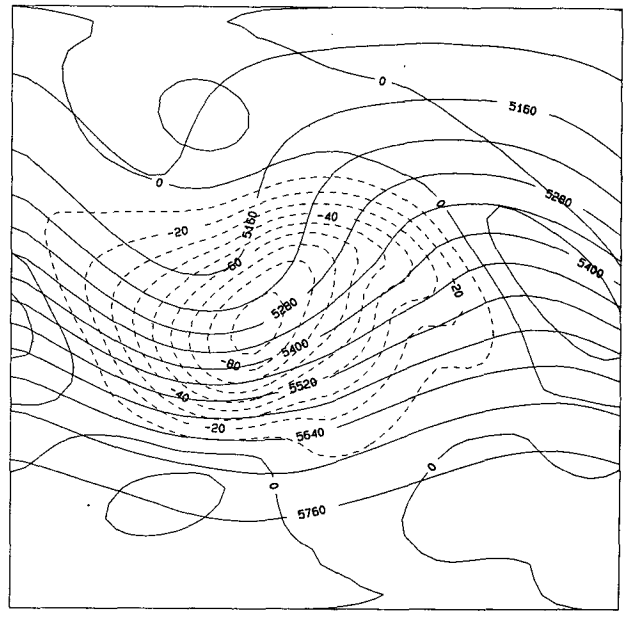

FIG. 8. The 500-mb geopotential height (m, solid) and 6-h height tendency (m, dashed and solid) centered at 24 h in the simulation. Height contours are every 60 m and height tendency contours are every 10 m.

the diabatic forcing in the vertical component of the P vector would further increase the P-vector divergence in this region as it is above the level of maximum diabatic heating.

The P-vector divergence at the 900-mb level (Fig. 9), which is the lowest level that the three-dimensional P-vector divergence can be calculated, shows a strong relationship to the frontal troughs and the inverted trough to the northwest of the surface low. Ahead of both the warm and cold fronts, P-vector divergence is evident, which indicates that height falls are being forced in these regions. This is consistent with moving fronts. However, the overall pattern of height tendency forcing near the surface does not give a clear picture of the likely height tendency for the low pressure center. The observed sea level pressure tendency over the 6-h period centered on the forcing is shown in Fig. 10. Similar to what was observed at 500 mb, the observed pressure tendency has a broad region of pressure falls centered near the low center, with several axes of relatively strong pressure tendencies indicated, which produces an asymmetric pattern. The axes of larger pressure falls correspond very well with the regions of strongest P-vector divergence even though the large-scale pattern differs substantially from the observed pressure tendency. The discrepancy in this case is the result of both being near the boundary and not inverting the Laplacian operator. At the boundary, the solution for the geopotential tendency is subject to the boundary condition given in (2.11b), which depends upon the sign of P_3. Consequently, warm and cold thermal advection at the surface can alter the low-level tendency for the same profile of P-vector forcing. Considerable care must be taken when attempting to interpret the P-vector divergence as a height tendency, particularly near the surface.

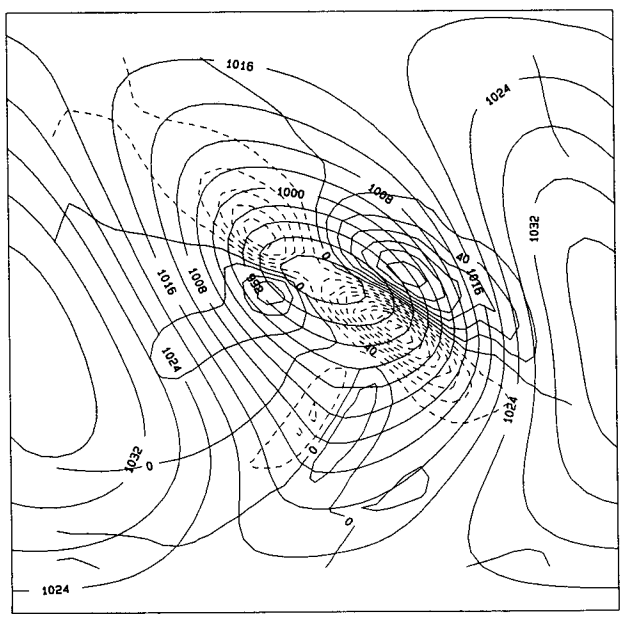

FIG. 9. Same as Fig. 7 except for sea level pressure and P vectors at 950 mb.

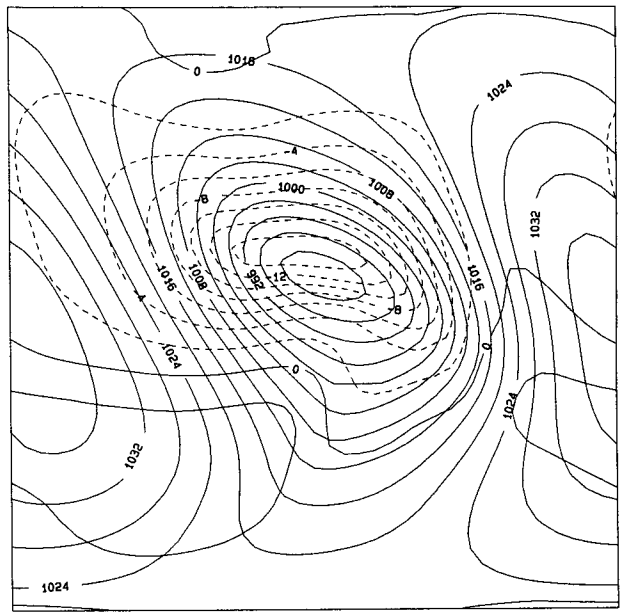

FIG. 10. Same as Fig. 8 except for sea level pressure (mb) and pressure tendency (mb).

The P-vector divergence shown in Fig. 7 can alternatively be interpreted from the perspective of the advection of quasigeostrophic potential vorticity as indicated by (2.12). This perspective avoids the difficulty in trying to interpret the forcing as the inverse of the response as suggested above for the geopotential tendency. Given no diabatic generation of potential vorticity, the local quasigeostrophic potential vorticity tendency is simply given by the advection of the potential vorticity. Consequently the propagation of a quasigeostrophic potential vorticity maxima can be directly deduced from the P-vector divergence. From this perspective, the positive-valued regions of P-vector divergence in Fig. 7 correspond to regions of cyclonic potential vorticity advection, where the potential vorticity should increase with time. The distribution of quasigeostrophic potential vorticity at 500 mb (not shown) is very similar to the distribution of absolute vorticity shown in Fig. 2. Again the eastward propagation of the trough is indicated by the positive (negative) potential vorticity advection downstream (upstream) from the potential vorticity maxima in the trough. This is consistent with the deduced height falls obtained from the geopotential tendency perspective. However, the magnitude of the quasigeostrophic flow changes associated with a given quasigeostrophic potential vorticity distribution also requires the inversion

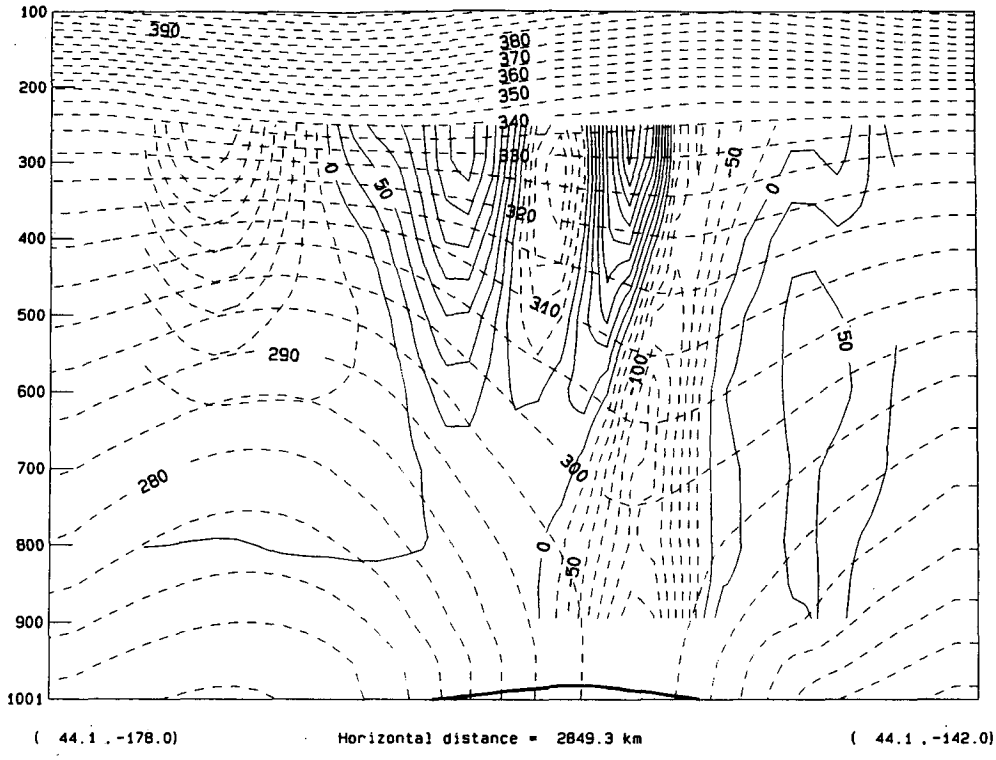

FIG. 11. West–east cross section of three-dimensional P-vector divergence (solid and dashed) and potential temperature (K, dashed) through center of cyclone. Potential temperature is contoured every 5 K. The P-vector divergence is in 1.5×10^{14} m s^{-1}, which is equivalent to meters per hour for a 4000-km-wavelength wave. Solid lines correspond to P-vector divergence and dashed lines to P-vector convergence.

of a Poisson equation, which is equivalent to solving for the height tendency from the forcing.

A similar interpretation of the low-level P-vector divergence is possible and avoids the boundary problem that occurs with the geopotential tendency. Since the significant values of quasigeostrophic potential vorticity are essentially confined to the frontal regions and the low center, the regions of large P-vector divergence in Fig. 9 suggest the rotation of the fronts around the low center as well as eastward movement of the low itself. The strongest P-vector divergence to the east of the low center corresponds to the direction that the low and potential vorticity maxima subsequently move. This propagation can be deduced without regard to the actual height tendency, which could even be a height increase.

The potential vorticity perspective is perhaps most enlightening when examining the vertical structure of the P-vector divergence. Figure 11 shows the P vector divergence along the west–east cross section through the center of the cyclone. As discussed above, the movement of the potential vorticity maxima is evident through the depth of the troposphere. Both the eastward propagation of the upper-level trough and the surface cyclone are clearly indicated in this cross section. It is interesting to note that geostrophic potential vorticity advection ($-\mathbf{V}_g \cdot \nabla_H q$) appears as two separate columns, one associated with the upper trough and one with the surface low. This suggests that the upper- and lower-level disturbances are not directly coupled. The region of potential vorticity advection associated with the surface low reflects the impact of diabatic processes acting prior to this time and could be stronger had the diabatic forcing been included in the P-vector diagnosis. Further insight can be obtained by recognizing that adiabatic motion along the potential temperature surfaces in the cross section is bringing the upper-level high potential vorticity air into a region of lower static stability. This indicates that the upper-level trough will intensify assuming that the potential vorticity is conserved.

c. *Ageostrophic circulation and P vectors*

The final aspect of P-vector diagnosis comes from their relationship to the ageostrophic circulation of the synoptic-scale wave. As mentioned in the last section, the ageostrophic circulation can be considered as composed of a contribution by the advection of geostrophic momentum and a contribution by the isallobaric wind. Lim et al. (1991) suggest that the advective contribution dominates at upper levels, while the

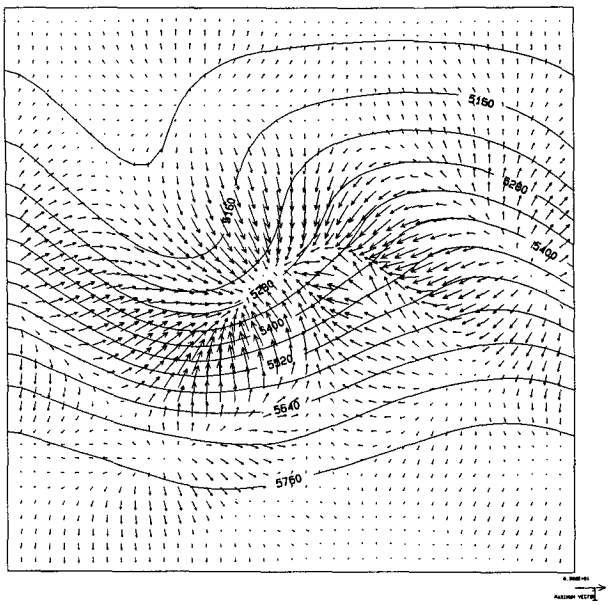

FIG. 12. The 500-mb geopotential height (m, solid) and isallobaric wind vectors (m s^{-1}) at 500 mb. Isallobaric wind vectors are scaled according to magnitude. Maximum vector appears in lower right corner and corresponds to 9 m s^{-1}.

two are comparable in magnitude at lower levels. To verify the relative magnitudes of the forcing terms for the ageostrophic circulation, the isallobaric wind was calculated from the observed 3-h height tendencies in the model. The 500- and 950-mb isallobaric winds for the three hours prior to the time of *P*-vector forcing are shown in Figs. 12 and 13 and the advectively forced winds (*P* vectors) are shown in Figs. 3 and 4. A comparison of these figures reveals that the advective contribution tends to dominate the isallobaric contribution at both 500 mb and 950 mb. At 500 mb the *P* vectors are larger by a factor of 3 compared to the isallobaric winds, while at 950 mb the *P* vectors are larger by only a factor of 2 in the frontal regions and less elsewhere. This differs from the results of Lim et al. (1991) at the lower levels, which is probably due to the considerably more intense smaller-scale features in this case compared to the large-scale mean fields examined by Lim et al. (1991). The present results suggest that the geostrophic advection of geostrophic momentum is the most significant factor in forcing the ageostrophic circulation of an intensifying cyclone with strong frontal features.

Although the magnitude of the advective contribution to the ageostrophic circulation indicates its dominance, the structure of the isallobaric and advective contributions relative to each other plays a significant role in determining the actual ageostrophic circulation. Lim et al. (1991) discuss how the isallobaric contribution tends to cancel the meridional component of the advective contribution aloft to result in a zonal dominance in the ageostrophic flow at upper levels. At lower levels, Lim et al. (1991) indicate that just the opposite occurs so the zonal components cancel to result in a primarily meridional ageostrophic flow. This effect at upper levels can be seen for the present wave by comparing the *P* vectors at 500 mb in Fig. 3 to the isallobaric wind at 500 mb in Fig. 12. The isallobaric winds are strongly divergent and are directed into the height fall center, while the *P* vectors tend to be more rotational and are in phase with the wave. The result is that downstream from the trough the isallobaric wind tends to cancel the *P* vectors on the anticyclonic side of the jet and weakly reinforce them on the cyclonic side. In the trough and the ridge, the two flows tend to be oriented along the jet but oppose each other to reduce the *P*-vector contribution to the ageostrophic flow. The observed ageostrophic flow at 500 mb is shown in Fig. 14 and indicates that the strongest ageostrophic flow is zonally directed in the trough and downstream ridge. Near the surface, the isallobaric wind (Fig. 13) is directed into the pressure fall center, which is displaced slightly to the northeast of the low pressure center. The *P* vectors (Fig. 4) are essentially parallel to the isobars and strongest across the fronts and inverted trough. At this level, the effect of the isallobaric contribution is to force the ageostrophic flow into the low center, particularly along the fronts and inverted trough where the *P* vectors point across the front or trough axis. In the frontal and inverted trough region, the *P* vectors or advective contribution seem to represent the ageostrophic flow associated with the two-dimensional frontal processes

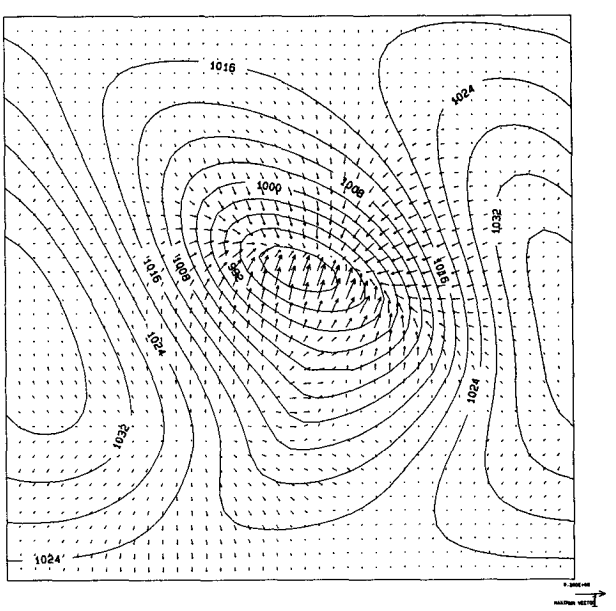

FIG. 13. Same as Fig. 12 except for sea level pressure and isallobaric wind vectors at 950 mb. Maximum vector corresponds to 20 m s^{-1}.

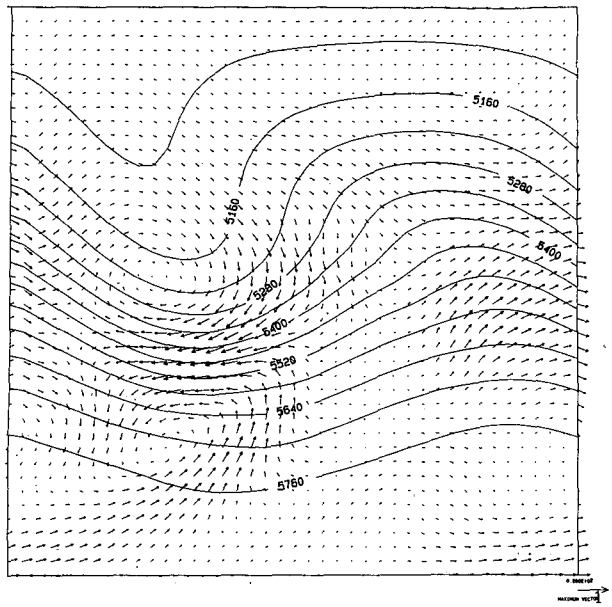

FIG. 14. The 500-mb geopotential height (m, solid) and ageostrophic wind vectors at 500 mb. Ageostrophic wind vectors are ($m\ s^{-1}$) and scaled according to magnitude. Maximum vector appears in lower right corner and corresponds to 20 $m\ s^{-1}$.

while the isallobaric contribution seems to represent the contribution due to cyclone-scale processes. This partitioning is evidently due to the small-scale structure of the frontal troughs, which is due to boundary layer and frontogenetical processes that do not directly contribute to the larger-scale pressure changes associated with the wave.

Although the P vectors alone are insufficient to determine the actual ageostrophic circulation of a synoptic-scale wave, the isallobaric contribution can easily be determined from previous analyses or height tendency observations to estimate this contribution. Diagnosis of the ageostrophic circulation from the P vectors and the isallobaric wind is then possible. Partitioning the ageostrophic wind into the advective part (P vectors) and the local tendency (isallobaric wind) may be useful to understand the wave dynamics and life cycle of synoptic-scale systems.

4. Summary and concluding remarks

The work described here is an attempt to draw together the geostrophic forcing in the geopotential tendency and ω equations. The horizontal components of **P** are defined to be the advection of geostrophic momentum, and the vertical component of **P** is defined to be the temperature advection. The geopotential tendency equation can then be derived with the three-dimensional divergence of the P vector on the right-hand side, which represents the geostrophic forcing of geopotential tendency. Consequently, the horizontal divergence of **P** is the geostrophic absolute vorticity advection, and the three-dimensional divergence of the P vector is the geostrophic quasigeostrophic potential vorticity advection. The P vector is related to the Q vector, C vector, and ageostrophic circulation. With the scaling factors of f_0 and σ in the definition of the curl, the horizontal components of the curl of **P** is perpendicular and proportional to the **Q**. The vertical component of the curl of **P** is the ageostrophic pseudovorticity or vertical component of the C vector. The ageostrophic wind can be partitioned into the P vector (geostrophic advective) and the isallobaric wind contributions. Finally, we note that the diabatic effect can be easily incorporated into the P-vector formulation by adding the apparent heat source to the P_3 component when the release of latent heat is important.

Application of the P-vector diagnostics to an example of an idealized midlatitude cyclone indicate that the P vectors provide useful insight into the synoptic-scale dynamics. The interpretation of the P-vector divergence as height tendency forcing or quasigeostrophic potential vorticity advection allows diagnosis of the propagation and cyclonic spinup of the system. Solution for the actual height tendency or the resultant geostrophic circulation from the potential vorticity requires the solution of an elliptic equation, which could be done. However, useful insight into the wave propagation was obtained from the forcing alone. The distribution of the P vectors in both the horizontal and the vertical provided a clear representation of all the geostrophic forcing of the wave. In the horizontal, the P vectors were interpreted from the perspective of the advection of geostrophic momentum, which indicates the propagation of the wave. In the vertical, the P vectors were interpreted from the perspective of thermal advection, which allows deduction of the vertical motion and differential thermal advection that will alter the geopotential height field. Combined with an estimate of the isallobaric wind, the P vectors were shown to be useful in diagnosing the ageostrophic flow. Although the dynamics and ageostrophic circulation of synoptic-scale waves can be obtained from traditional forms of the geopotential tendency and other equations, the P-vector representation seems to provide a useful presentation of the dynamic forcing in a single quantity, which results in a unified physical interpretation of the dynamics.

Acknowledgments. The authors are grateful to Professors Richard Johnson and J. J. Toth for their valuable comments. The suggestions of Qin Xu, Wayne Schubert, and another anonymous reviewer on this manuscript were extremely valuable and are gratefully acknowledged. This work was supported by NSC82-0202-M-002-073 from National Research Council of Taiwan.

REFERENCES

Berrisford, P., J. C. Marshall, and A. A. White, 1993: Quasigeostrophic potential vorticity in isentropic coordinates. *J. Atmos. Sci.*, **50**, 778–782.

Davis, C. A., and K. A. Emanuel, 1991: Potential vorticity diagnostics of cyclogenesis. *Mon. Wea. Rev.*, **119**, 1929–1953.

Haynes, P. H., and M. E. McIntyre, 1987: On the evolution of vorticity and potential vorticity in the presence of diabatic heating and frictional or other forces. *J. Atmos. Sci.*, **44**, 828–841.

Holton, J. A., 1979: *An Introduction to Dynamic Meteorology.* Academic Press, 391 pp.

Hoskins, B. J., 1975: The geostrophic momentum approximation and the semi-geostrophic equations. *J. Atmos. Sci.*, **32**, 233–242.

——, 1982: The mathematical theory of frontogenesis. *Ann. Rev. Fluid Mech.*, **14**, 131–151.

——, and F. P. Bretherton, 1972: Atmospheric frontogenesis models: Mathematical formulation and solution. *J. Atmos. Sci.*, **29**, 11–37.

——, and I. Draghici, 1977: The forcing of ageostrophic motion and according to the semi-geostrophic equations and in an isentropic coordinate model. *J. Atmos. Sci.*, **34**, 1859–1867.

——, and M. A. Pedder, 1980: The diagnosis of middle latitude synoptic development. *Quart. J. Roy. Meteor. Soc.*, **106**, 707–719.

——, I. Draghici, and H. C. Davies, 1978: A new look at the omega equation. *Quart. J. Roy. Meteor. Soc.*, **104**, 31–38.

Keyser, D., B. D. Schmidt, and D. G. Duffy, 1992: Quasigeostrophic vertical motion diagnosed from along- and cross-isentropic components of the **Q** vector. *Mon. Wea. Rev.*, **120**, 731–741.

Lim, G. H., J. R. Holton, and J. M. Wallace, 1991: The structure of the ageostrophic wind field in baroclinic waves. *J. Atmos. Sci.*, **48**,1733–1745.

Nuss, W. A., and R. A. Anthes, 1987: A numerical investigation of low-level processes in rapid cyclogenesis. *Mon. Wea. Rev.*, **115**, 2728-2743.

Schubert, W. H., 1985: Semigeostrophic theory. *J. Atmos. Sci.*, **42**, 1770–1772.

Xu, Q., 1992: Ageostrophic pseudovorticity and geostrophic C-vector forcing—A new look at the **Q** vector in three dimensions. *J. Atmos. Sci.*, **49**, 981–990.

——, and D. Keyser, 1993: Barotropic and baroclinic ageostrophic winds and completeness of solution for the psi equations. *J. Atmos. Sci.*, **50**, 588–596.